An Experimental Estimation of Hybrid ANFIS–PSO-Based MPPT for PV Grid Integration Under Fluctuating Sun Irradiance

Priyadarshi, Neeraj; Sanjeevikumar, Padmanaban; Holm-Nielsen, Jens Bo; Blaabjerg, Frede; Sagar Bhaskar, Mahajan

Published in:
I E E E Systems Journal

DOI (link to publication from Publisher):
10.1109/JSYST.2019.2949083

Publication date:
2020

Document Version
Accepted author manuscript, peer reviewed version

An Experimental Estimation of Hybrid ANFIS–PSO-Based MPPT for PV Grid Integration Under Fluctuating Sun Irradiance

Neeraj Priyadarshi, *Member, IEEE*, Sanjeevikumar Padmanaban, *Senior Member, IEEE*, Jens Bo Holm-Nielsen, Frede Blaabjerg, *Fellow, IEEE*, and Mahajan Sagar Bhaskar, *Member, IEEE*

***Abstract*—To enhance the photovoltaic (PV) power-generation conversion, maximum power point tracking (MPPT) is the foremost constituent. This article introduces an adaptive neuro-fuzzy inference system–particle swarm optimization (ANFIS–PSO)-based hybrid MPPT method to acquire rapid and maximal PV power with zero oscillation tracking. The inverter control strategy is implemented by a space vector modulation hysteresis current controller to get quality inverter current by tracking accurate reference sine-shaped current. The ANFIS–PSO-based MPPT method has no extra sensor requirement for measurement of irradiance and temperature variables. The employed methodology delivers remarkable driving control to enhance PV potential extraction. An ANFIS–PSO-controlled Zeta converter is also modeled as an impedance matching interface with zero output harmonic agreement and kept between PV modules and load regulator power circuit to perform MPPT action. The attainment of recommended hybrid ANFIS–PSO design is equated with perturb and observe, PSO, ant colony optimization, and artificial bee colony MPPT methods for the PV system. The practical validation of the proposed grid-integrated PV system is done through MATLAB interfaced dSPACE interface and the obtained responses accurately justify the proper design of control algorithms employed with superior performance.**

***Index Terms*—adaptive neuro-fuzzy inference system–particle swarm optimization (ANFIS–PSO), fuzzy logic control (FLC), maximum power point tracking (MPPT), photovoltaic (PV) system, space vector modulation hysteresis current controller (SVMHCC), Zeta converter.**

NOMENCLATURE

I_{phot}	Photocurrent.
I_{RSC}	Reversed saturating current.
V_{Thm}	Thermal voltage.
G_S	Sun insolation.
T_{cell}	PV cell temperature.
$I_{\text{short\_Ref}}$	PV cell short-circuit current at STC.
STC	Standard test conditions.
K_{sc}	Coefficient of short current.
$T_{\text{cell\_Ref}}$	PV cell temperature at 25 °C.
G_{Ref}	1000 W/m^2.
$I_{\text{RS\_Ref}}$	Reverse saturation current at STC.
E_B	Bandgap.
K_{BC}	Boltzmann's constant.
QE	Charge on electron.
D_{duty}	Duty cycle.
ΔV_{ripple}	Ripple in voltage.
ΔI_{ripple}	Ripple in current.
V_{PV}	PV voltage.
V_{out}	Output voltage.
$f_{\text{switching}}$	Switching frequency.
L_A, L_B	Inductors.
C_A,C_B	Capacitors.
p_j, r_j, b_j	Parameters of the membership function.
T	Functional current.
T_0	Center axis function.

Manuscript received November 19, 2018; revised February 8, 2019, April 26, 2019, and August 26, 2019; accepted September 23, 2019. *(Corresponding author: Sanjeevikumar Padmanaban.)*

N. Priyadarshi is with the Department of Electrical Engineering, Brisa Institute of Technology (Trust), Ranchi, 835217, India (e-mail: neerajrjd@gmail.com).

S. Padmanaban and J. B. Holm-Nielsen are with the Center for Bioenergy and Green Engineering, Department of Energy Technology, Aalborg University, Esbjerg 6700, Denmark (e-mail: san@et.aau.dk; jhn@et.aau.dk).

F. Blaabjerg is with the Center of Reliable of Power Electronics, Department of Energy Technology, Aalborg University, Aalborg 9220, Denmark (e-mail: fbl@et.aau.dk).

M. S. Bhaskar is with the Renewable Energy Lab, Department of Communications and Networks Engineering, College of Engineering, Prince Sultan University, Riyadh 12435, Saudi Arabia (e-mail: sagar25.mahajan@gmail.com).

Digital Object Identifier 10.1109/JSYST.2019.2949083

I. INTRODUCTION

BY VIRTUE of depletion of traditional energy sources, the requisition and applications of renewable energy sources are booming globally. Amid entire renewable sources, the photovoltaic (PV) system has exceptional progression since the last decade [1]–[3]. By means of nonlinear voltage/current features of PV modules, the transfiguration competency is limited. Maximum power point trackers (MPPTs) are imperative ingredients to warrant superlative PV energy generation under global power point tracking state [4]–[6]. In [4]–[6], many MPPT control strategies have been inspected in the literary work. Perturb and observe (P&O), Hill climbing (HC), and incremental conductance (INC) are reviewed as classical MPPT methods [7]–[9]. The hardware implementation of P&O and HC methods is simpler, but it comprises high oscillations nearer to a maximum power point (MPP), which results in power losses. The INC method is accurate and flexible under fluctuating atmospheric situations. Nevertheless, it contains simulation and experimental complexities. However, the above-mentioned algorithms are not efficient under varying solar irradiance and for the calculation

of correct perturbation size. Therefore, intelligent fuzzy logic control (FLC) and artificial neural network (ANN) techniques as MPPT trackers are selected to rectify classical MPPT algorithms' deficiency under fluctuating weather conditions [10]. Various research teams are working to achieve low cost and improve tracking efficiency and reliability of PV-based industrial sectors. In this regard, the fuzzy logic-based MPPT approach plays a vital role as it has simpler architecture and robust design that is able to solve uncertainties and nonlinearity problems of the PV power system. However, expert knowledge and design of rule base systems are the key challenges for FLC design. Compared to classical algorithms of MPPT techniques, the ANN method consisting of multilayered neurons is widely employed for fast PV power tracking under changing environmental conditions. However, using this method large data is required for proper training, periodically to achieve an accurate MPPT. After combining ANN and FLC, the hybrid algorithm comprises attractive learning abilities that provide trained membership for MPPT action. It is also noted that there is a requirement to calculate PV voltage and current to implement MPPT algorithms. However, some MPPT controllers failed because of high hardware complexity and noise calculations.

Here, a hybrid adaptive neuro-fuzzy inference system (ANFIS) occupying peak power tracker is adopted, that subsists the benefit of couple algorithms [11]. The training and updation of ANFIS specifications are a challenging task for the designers. The recent artificial intelligent algorithms, such as particle swarm optimization (PSO), firefly algorithm, artificial bee colony (ABC), and ant colony optimization (ACO), are used to solve optimized problems [12]–[15]. The FLC and ANN provide better PV tracking ability under uniform variation of Sun insolation level. However, under changing weather conditions where multiple peaks are present and it is very difficult to obtain the MPP region, PSO provides an optimal solution as it requires very few parameters for adjustment. Compared to the mentioned optimization algorithms, the PSO method has a low sampling point, simpler mathematical analysis, easy hardware implementation, and economical computing estimation and provides fast and accurate PV power tracking under varying operating conditions. In contrast to the gradient techniques, the PSO provides simpler and rapid updation convergence velocity [16]. Moreover, the PSO does not need initial parameter calculation and there is no requirement of learning rate. It delivers rapid convergence velocity, simpler construction, and easy employment with utmost PV tracking efficiency utilization. This research work delivers effective, simpler, and robust hardware implementation of MPPT circuitry. When equated with the classical dc–dc converter, a Zeta converter provides low voltage ripple in voltage yield [17]. Compared to other power converters, the Zeta converter has attractive characteristics as it transforms power in a single stage, consists of naturally isolating design, provides power factor corrections, and works in the step-up/down mode of operation. It is also termed as the fourth-order nonlinear power converter working in continuous/discontinuous modes.

Numerous inverter current mechanisms, namely, predictive current controller [18], hysteresis current controller (HCC) [19], space vector pulsewidth modulation (SVPWM) [20], etc., have been used to control inverters. In the predictive controller method, the measured current should be identical to the reference current by controlling inverter voltage. This method comprises complicated controller architecture with invariable switching periodicity and has varying loading behavior. Gating signals to the inverter are produced by application of boundary bands as far as the HCC method is considered. Nevertheless, HCC has varying switching behavior as the main deficiency. SVPWM uses simpler mapped methodology with minimum switching losses, has linear nature of modulation index, and has minimal harmonic contents. In contrast to HCC, SVPWM has a phase-locked loop as an additional component, which produces sluggish dynamic responses. Hence, a requisite inverter controller is recommended that comprises all benefits of SVM and HCC and has a simpler implementation with least switching losses. The rapid and extant three-phase inverter is composed using a space vector modulation hysteresis current controller (SVMHCC). It consists of benefits of both SVM and HCC and delivers high dynamicity, which improves the system pursuance. Hence, the proposed SVMHCC method comprising robust dynamic response is the gratification of this technique. In [21], the ANFIS–PSO-based methodology for estimation of gas density and the obtained responses are equated with three different approaches. However, the gas density has been estimated using a graphical and statistical approach. In [22], the hydrocarbons' interfacial tension is predicted using the ANFIS–PSO approach. However, the proposed algorithm with experimental estimation is not addressed. In [23], a genetic algorithm (GA)–PSO–ANFIS-based strategy is discussed for forecasting electricity production using a PV-based microgrid. Nevertheless, the investigation for MPPT and grid connection is not validated experimentally. In [24], the PSO–ANFIS method is presented for forecasting short-term PV power generation using microgrid applications. However, the MPPT and grid synchronization approach for the PV grid-integrated system is not discussed. Moreover, the application of the hybrid ANFIS–PSO approach has not been discussed and compared with PSO, ACO, and ABC algorithms in the literature for PV grid integration. In [25], a reinforcement learning-based online controller has been discussed for a static compensator distributor that provides a solution for power quality challenges in microgrid systems. It can use voltage and current variables for compensation of harmonic distortion, unbalanced loading current, and reactive power for microgrid systems. The employed online control used for stand-alone microgrid systems (weak ac) has been analyzed using a simulation environment under various loading and faulty operating conditions. In [26], the hybrid GA–PSO method has been presented for lower frequency oscillation damping for improvement of stability issues of the multimachine power system. The major objective of hybrid techniques is to provide reduction of fuzzy calculations and uncertainties. In this approach, the employed controller has been optimized offline using hybrid methods. The England 10-unit, 39 bus-based power system has been realized using simulation to validate the effectiveness of the hybrid technique that comprises flexible control and simpler implementation under varying loading and faulty operating conditions.

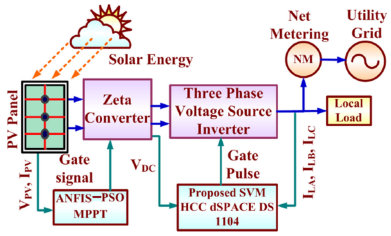

Fig. 1. Hybrid ANFIS–PSO-based PV grid integration system.

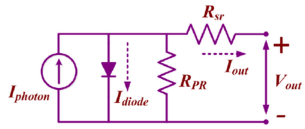

Fig. 2. Equivalent PV cell model.

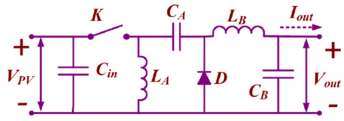

Fig. 3. Power circuit of a Zeta converter.

At present, efficiency of the renewable power system is the major concern that belongs to optimization issues and blooming analyzing ground for the academia. The industry experts are unable to discuss the detailed mathematical formulation of the given optimization problems. The possible solution of optimization problems can be obtained by integrating academia learning to industrial sector applications. In light of the above discussion, the main contribution of this article is as follows. The proposed hybrid ANFIS–PSO-based MPPT algorithm has been implemented for PV MPPT functioning and grid integration. The performance of the proposed hybrid ANFIS–PSO algorithm is equated with PSO, ACO, and ABC algorithms under low/high solar insolation profile and in partial shading conditions. The proposed scheme provides a rapid convergence velocity, low MPPT tracking period, zero steady-state error, and high PV tracking efficiency compared to recent optimized PSO, ACO, and ABC algorithms. The attainment of PV grid generation has been realized and verified through practical emanation of hybrid ANFIS–PSO with SVMHCC inverter control using dSPACE (DS 1104) interface with fluctuating Sun irradiance.

The rest of the article is organized as follows. Section II provides the overall structure of the proposed PV integration system to the grid. The SVMHCC inverter control with its peculiarity is discussed in Section III. The experimental analysis and investigation results are discussed in Section IV. Finally, a conclusion is provided in Section V based on the investigation.

II. Description of the Proposed PV System

Fig. 1 demonstrates the structural view of the hybrid ANFIS–PSO-based PV grid integration system. A Zeta converter controlled by a hybrid PSO–ANFIS algorithm with SVMHCC inverter control has been implemented for optimal PV power capture with smooth inverter control. The impedance balancing performance is executed by the Zeta converter that is placed between solar modules and inverter. Pure sine wave as an inverter output is supplied to the electrical grid using the proposed control methodology.

A. PV Generator Modeling

A PV cell model is shown in Fig. 2. The equivalent model of PV cell comprises a current source, a diode, and series/parallel resistances. The mathematical equations describing the electrical circuits can be derived as

$$I_{\text{out}} = I_{\text{phot}} - I_{\text{diode}} = I_{\text{phot}} - I_{\text{RSC}}\left[\exp\left(\frac{V_{\text{out}}}{V_{\text{Thm}}}\right) - 1\right] \tag{1}$$

where I_{phot} is the photocurrent, I_{RSC} is the reversed saturating current, and V_{Thm} is the thermal voltage. Photon current is expressed linearly with Sun insolation (G_s) and PV cell temperature (T_{cell}) as follows:

$$\begin{aligned} I_{\text{photon}} &= \left[I_{\text{short\_Ref}} + K_{\text{sc}}\left(T_{\text{cell}} - T_{\text{cell\_Ref}}\right)\right]\frac{G_s}{G_{\text{Ref}}} \\ &= f\left(G_s, T_{\text{cell}}\right) \end{aligned} \tag{2}$$

where $I_{\text{short\_Ref}}$ is the PV cell short-circuit current at STC (standard test conditions), K_{sc} is the coefficient of short current, $T_{\text{cell\_Ref}}$ is the PV cell temperature at 25 °C, G_S is the Sun irradiance, and G_{Ref} is 1000 W/m^2. Also, the diode current is expressed as

$$\begin{aligned} I_{\text{diode}} &= \left[\begin{array}{l} I_{\text{RS\_Ref}}\left(\dfrac{T_{\text{cell}}}{T_{\text{cell\_Ref}}}\right)^3 \\ \times\exp\left\{\dfrac{\text{QE}\times E_B}{K_{\text{BC}}\times A_d}\left(T_{\text{cell\_Ref}}^{-1} - T_{\text{cell}}^{-1}\right)\right\} \\ \times\left\{\exp\left(\dfrac{\text{QE}\times V_{\text{out}}}{K_{\text{BC}}\times A_d\times T_{\text{cell}}}\right) - 1\right\} \end{array}\right] \\ &= f\left(V_{\text{out}}, T_{\text{cell}}\right) \end{aligned} \tag{3}$$

where $I_{\text{RS\_Ref}}$ is at STC (reverse saturation current), E_B is the bandgap, K_{BC} is Boltzmann's constant, and QE is the charge on electron.

Finally, the PV cell current can be expressed as

$$I_{\text{out}}\left(V_{\text{out}}, G_s, T_{\text{cell}}\right) = f\left(G_s, T_{\text{cell}}\right) - f\left(V_{\text{out}}, T_{\text{cell}}\right). \tag{4}$$

B. Zeta Converter

The Zeta converter (depicted in Fig. 3) is treated as the fourth-order switching power converter containing two capacitors and two inductors as main components. When equated with a buck/boost converter, it generates noninverting outcomes and works under continuous and discontinuous states while the mode

TABLE I
ZETA CONVERTER SPECIFICATIONS

Parameters	Value
Inductors (L_A, L_B)	0.5 mH, 0.6 mH
Capacitors (C_A, C_B)	800 µF, 1000 µF
Switched frequency ($f_{switching}$)	6 kHz
Ripple current (ΔI_{ripple})	2.5 A
Ripple voltage (ΔV_{ripple})	6x10^{-2} V

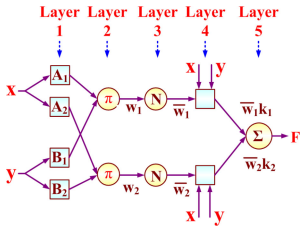

Fig. 4. Architecture of an ANFIS controller.

of operation with continuous operation is frequently acceptable. Table I presents the used specifications of the Zeta converter design. The mathematical equations governing the design of Zeta parameters are mentioned as follows:

$$\left.\begin{aligned} V_{\text{out}} &= V_{\text{PV}}\left(\frac{D_{\text{duty}}}{1-D_{\text{duty}}}\right) \\ L_A = L_B &= \frac{V_{\text{PV}}V_{\text{out}}}{\Delta I_{\text{ripple}} f_{\text{switching}}(V_{\text{PV}}+V_{\text{out}})} \\ C_A = C_B &= \frac{I_{\text{out}}V_{\text{out}}}{\Delta V_{\text{ripple}} f_{\text{switching}}(V_{\text{PV}}+V_{\text{out}})} \end{aligned}\right\} \quad (5)$$

where D_{duty} is the duty cycle, ΔV_{ripple} is the ripple in voltage, ΔI_{ripple} is the ripple in current, V_{PV} is the PV voltage, V_{out} is the output voltage, $f_{\text{switching}}$ is the switching frequency, L_A and L_B are inductors, and C_A and C_B are capacitors.

C. Hybrid ANFIS–PSO-Based MPPT Controller

The training and updation of ANFIS specifications are a challenging task for the designers nowadays. Compared to the gradient techniques, the PSO provides simpler and rapid updation convergence velocity [16]. Moreover, the PSO does not require initial parameter calculation and nor there is requirement of a learning rate. Fig. 4 depicts the architecture of the ANFIS controller and comprises antecedent and conclusions as a major component with five total layers. The mathematical equations associated with multilayer feedforward network are as follows:

$$W_j = \mu_{P_j}(x) * \mu_{Q_j}(y), \quad \bar{W}_j = \frac{W_j}{W_1+W_2}, \quad j = 1,\ 2. \quad (6)$$

K_1, K_2, and K can be expressed as follows:

$$\left.\begin{aligned} K_1 &= A_1x + B_1y + R_1z, \quad K_2 = A_2x + B_2y + R_2z \\ K &= \frac{W_1K_1 + W_2K_2}{W_1+W_2} = \bar{W}_1K_1 + \bar{W}_2K_2 \end{aligned}\right\}. \quad (7)$$

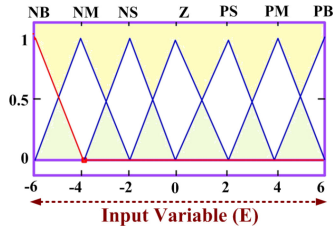

Fig. 5. Membership functions' input framework (E).

The membership function (bell-shaped) lies between 0 and 1 and is evaluated mathematically as

$$\left.\begin{aligned} \mu_{P_j}(x) &= \frac{1}{1+\left[\left((x-r_j)p_j{}^{-1}\right)^2\right]^{bj-3}} \\ \mu_{P_j}(x) &= \exp\left[-\left[\left(\frac{x-r_j}{p_j}\right)^2\right]^{bj}\right] \end{aligned}\right\} \quad (8)$$

where p_j, r_j, and b_j are the parameters of the membership function.

Based on the above equations, the antecedent component has p_j, r_j, and b_j as trainable values. Let a_j, b_j, and c_j are trained values in conclusion components. The total membership in the conclusion component comprises each chromosome equal to $(N+1)$ S, where N is the total data input and S is the number of rule base. So, the value of the fitness expression has been estimated with root mean square error (RMSE) [21], [22], [24].

The inference rule base has been designed by collecting input/output parameters that are tuned using the back-propagation method. The fuzzy inference system is able to control imprecision as well as uncertainty and has been designed by the trial-and-error method for optimal working. Crisp variables are transformed into fuzzy values by considering membership functions. In this work, the number of membership functions and their corresponding values depend on data collections of the PV power system. The building components of a fuzzy logic controller directly affect the fuzzy inference systems. The trial-and-error approach has been employed to decide the shape of membership functions and there is no fixed technique for deciding the number of membership functions. However, membership functions lie between 0 and 1. The type of membership function does not affect the system performance. Nevertheless, the number of membership functions greatly affects the model performance, which evaluates the computational period and comprises multiple subsets of several linguistic variables.

Fig. 5 portrays the allocated membership values of error, which have seven linguistic shifting. The composition of max–min Mamdani's methodology in the act of inference rule decided by 49 fuzzy rules is described in Table II.

The behavior of a fuzzy system depends on inference rule and membership function, which are also based on a hit-or-miss process. The evaluation of these methods is period immoderate as well as imperceptive of parameter adaptation. On the other hand, ANN techniques are based on learned data and different layers. Nevertheless, insufficiency of rules to decide layer architecture is the major limitation of this method. Moreover, FLC and ANN are integrative intelligent techniques. An ANFIS

TABLE II
INFERENCE FUZZY DECISION

E / dE	NB	NM	NS	Z	PS	PM	PB
NB	Z	PB	Z	Z	NS	PB	PB
NM	PS	Z	NS	Z	NS	Z	NM
NS	NB	Z	PB	PS	PS	PS	PS
Z	Z	PS	NM	Z	PS	Z	NS
PS	Z	NB	PB	NS	Z	Z	PS
PM	NS	NS	PS	Z	NS	PS	PB
PB	PS	PS	Z	NB	Z	PM	NB

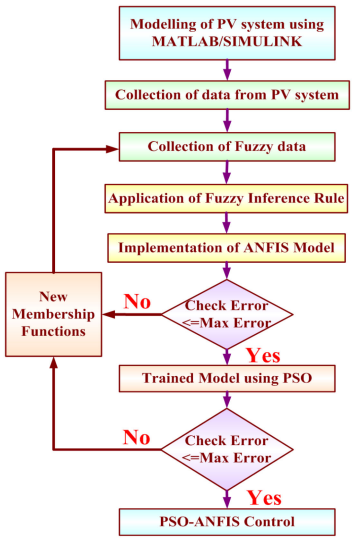

Fig. 6. Flowchart structure of an ANFIS–PSO-based MPPT control.

method is refined for inference rule base with learning data to minimize the computational period with factual modeling. The maximum error in the flowchart of Fig. 6 is 0.5 for 100 epochs of training data set. The mathematical relations present in [21], [22], and [24] have been used to calculate the maximum error value.

Unlike traditional MPPT controllers, this control has peak maximum power tracking, fast dynamicity, rapid velocity of convergence, and simpler contraption. Fuzzification, inference engine, and defuzzification are the premier process blocks of this algorithm. The MATLAB/Simulink model of an ANFIS–PSO methodology in the presence of an input parameter (PV voltage/current) yields duty ratio as pulsewidth modulation (PWM) generated signal. The detailed flowchart structure of an ANFIS–PSO-based MPPT control is described in Fig. 6. An advanced hybrid ANFIS technique gathers the fuzzy data with trained learning rules for proper adjustment of membership values before error has been minimized to the merest amount. Whenever membership parameters are adapted, the learned system is equipped to work as a hybrid MPPT controller. During the defuzzification, the centroid process is applied for adopting the Zeta converter duty ratio that is calculated according to the flowchart shown in Fig. 6 and ANFIS–PSO parameters are given in Table III .

TABLE III
ANFIS–PSO PARAMETERS

Parameters	Value
Size of particle	50
No. of iterations	50
Weight of Inertia	0.8
No. of Epochs	100
Required data set	180
Membership functions	49

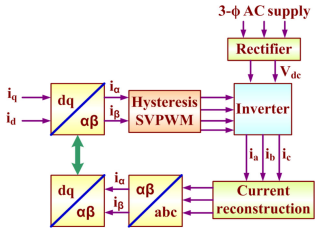

Fig. 7. Hysteresis SVPWM control.

Traditionally, the antecedent and consequent parameters are run separately. However, in this hybrid ANFIS–PSO approach, the entire parameters are simultaneously trained and mean square error has been minimized. The online learning has been evaluated to get adaptive learning rate of ANFIS architecture, which is derived using input/output parameters.

III. SVMHCC FOR INVERTER CURRENT CONTROL

The hysteresis current controller basically delivers instantaneous current corrections with highly accurate response and unrestricted system stability. However, the requirement of over-switched frequency of this approach can be compensated by combining it with space vector modulation. The SVMHCC-based inverter control provides proper switching sequence by adjusting hysteresis bands that produce compensating current as per reference current. The space vector modulation provides the maximum output voltage and reduction of switching frequencies compared to the conventional PWM approach. The proposed SVMHCC delivers less switch number and corrected components that are related to individual switching position. By application of the instantaneous reactive power method, the inverter reference current is produced. Real and apparent powers are being derived from the Clarke transformation. SVMHCC comprises supremacy of the coupled SVM and HCC approach. The produced error signal associates reference and measured compensator currents. The reference current vector region is determined by the hysteresis comparator as depicted with the block diagram in Fig. 7. Two band errors in Fig. 8 are directed to sector locator as well as switched functioning table [27], in accordance with the SVM method. This method combined the advantages of hysteresis and SVPWM simultaneously. HCC provides current-controlled strategy in which phase current has been evaluated as per the width of the hysteresis tolerance band. Three-phase currents (*a–b–c*) are transformed to two-phase

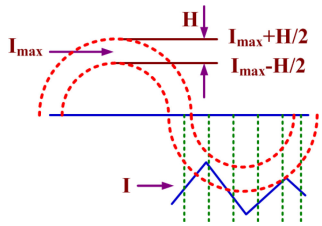

Fig. 8. Hysteresis band.

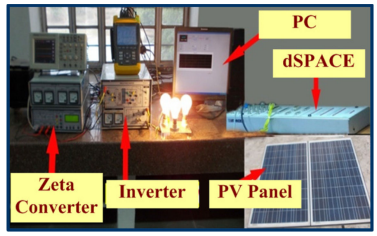

Fig. 9. Laboratory experimental setup of the hybrid ANFIS–PSO method integrated to grid.

(α–β) using the Clark transformation in Fig. 7.

$$\begin{bmatrix} T_\alpha & T_\beta & T_0 \end{bmatrix} = \begin{bmatrix} T_a & T_b & T_c \end{bmatrix} = \begin{bmatrix} 1 & 0 & \frac{1}{2} \\ \frac{-1}{2} & \frac{\sqrt{3}}{2} & \frac{1}{2} \\ \frac{-1}{2} & \frac{-\sqrt{3}}{2} & \frac{1}{2} \end{bmatrix} \quad (9)$$

where T is the functional current and T_0 is the center axis function. Again, d–q axis coordinates can be transformed to the α–β coordinate system as follows:

$$\begin{bmatrix} T_d & T_q & T_0 \end{bmatrix} = \frac{2}{3} \begin{bmatrix} T_\alpha & T_\beta & T_0 \end{bmatrix} \begin{bmatrix} \cos\cos\theta & -\sin\sin\theta & 0 \\ \sin\sin\theta & \cos\cos\theta & 0 \\ 0 & 0 & 1 \end{bmatrix}. \quad (10)$$

Gating signals are generated by supplying upper band output hysteresis comparing indicators AAU, ABU, and ACU and the lower band output signals AAL, ABL, and ACL to programmable logic array [27]. Inner-band signals have y_1, y_2, and y_3 outputs of V_k space vector. Six-region output of upper hysteresis band is given as follows:

$$\left.\begin{aligned} R_1 &= A_{AU}\bar{A}_{BU}\bar{A}_{CU}, & R_2 &= A_{AU}A_{BU}\bar{A}_{CU} \\ R_3 &= \bar{A}_{AU}A_{BU}\bar{A}_{CU}, & R_4 &= \bar{A}_{AU}A_{BU}A_{CU} \\ R_5 &= \bar{A}_{AU}\bar{A}_{BU}A_{CU}, & R_6 &= A_{AU}\bar{A}_{BU}A_{CU} \end{aligned}\right\}. \quad (11)$$

The output signal of the inner hysteresis band is derived as follows:

$$y_1 = \begin{pmatrix} R_1[A_{AL}\bar{A}_{BL}\bar{A}_{CL} + A_{AL}A_{BL}\bar{A}_{CL}] \\ +R_2A_{AL}A_{BL}\bar{A}_{CL} + R_5A_{AL}\bar{A}_{BL}A_{CL} \\ +R_6[A_{AL}\bar{A}_{BL}A_{CL} + A_{AL}\bar{A}_{BL}\bar{A}_{CL}] \end{pmatrix} \quad (12)$$

$$y_2 = \begin{pmatrix} R_1A_{AL}A_{BL}\bar{A}_{CL} + R_2[A_{AL}A_{BL}\bar{A}_{CL} \\ +\bar{A}_{AL}A_{BL}A_{CL}] + R_3[\bar{A}_{AL}A_{BL}\bar{A}_{CL} \\ +\bar{A}_{AL}A_{BL}A_{CL}] + R_4\bar{A}_{AL}A_{BL}A_{CL} \end{pmatrix} \quad (13)$$

$$y_3 = \begin{pmatrix} R_4\bar{A}_{AL}A_{BL}A_{CL} + R_4[\bar{A}_{AL}A_{BL}A_{CL} \\ +\bar{A}_{AL}\bar{A}_{BL}A_{CL}] + R_5[\bar{A}_{AL}\bar{A}_{BL}A_{CL} \\ +A_{AL}\bar{A}_{BL}A_{CL}] + R_6A_{AL}\bar{A}_{BL}A_{CL} \end{pmatrix}. \quad (14)$$

IV. Experimental Investigation

A. Experimental Setup

The grid PV system is modeled using Simulink and linked with dSPACE DS1104 board for performance verification. IGBT driver circuit, inverter, and PC with Fluke power quality analyzer as measuring devices are employed during practical justification of the PV system. The laboratory experimental setup of the hybrid ANFIS–PSO method integrated to grid is depicted in Fig. 9. The DS1104SL–DSP–PWM block is employed to produce the required PWM signal isolated with an optocoupler and supplied to Zeta converter's switch, as demonstrated in Fig. 10. Instantaneous power and PWM generation schemes for the hybrid ANFIS–PSO-based MPPT controller using dSPACE are shown in Fig. 10(a) and (b), respectively. The data acquisition and hybrid ANFIS–PSO MPPT algorithms have been interfaced using dSPACE DS1104 platform. LV25-P (voltage sensor), LA25-NP (current sensor), IRG4PH50U (IGBT), and RHRG30120 (diode) have been employed as major components. The proposed hybrid ANFIS–PSO method is implemented using MATLAB interfaced dSPACE platform in which supply signals (analog-to-digital converter (ADC) channel) are varying under the voltage range from -10 to $+10$ V. The output from the A/D channel is linked with a gain of 10 and passed through an analog filter that eliminates high-frequency noise signals. The instantaneous power has been evaluated by multiplying instant PV voltage/current. The proposed hybrid algorithm is implemented by providing inputs as instantaneous PV voltage and current, which produces power duty cycle for the Zeta converter.

B. Experimental Results and Discussion

Fig. 11(a) depicts the behavior of grid voltage/current through unity power factor condition under fluctuating Sun irradiance. The employed controllers trace upraised PV power and produce sine-shaped inverter current with high reaching preciseness. Fig. 11(b) describes the laboratory aftermath of inverter pursuance with negligible fluctuations under fluctuating Sun irradiance. With the aid of ANFIS–PSO and SVMHCC, the optimum designed PV generating system captures accurate active/reactive power with better precision. Practically found responses of inverter voltage/current, reveal that the pure sine signal is obtained with zero oscillation, as presented by Fig. 11(b). Practically obtained inverter voltage and current fast Fourier transform (FFT) spectra are illustrated in Fig. 12(a) and (b). Practical responses demonstrate the inverter voltage/current and grid voltage, which are in good agreement with the proposed SVMHCC controller design. It generates quality inverter current by tracking accurate reference sine-shaped current. The experimental results are quite satisfactory, as the IEEE 519 standard is followed by inverter voltage and current.

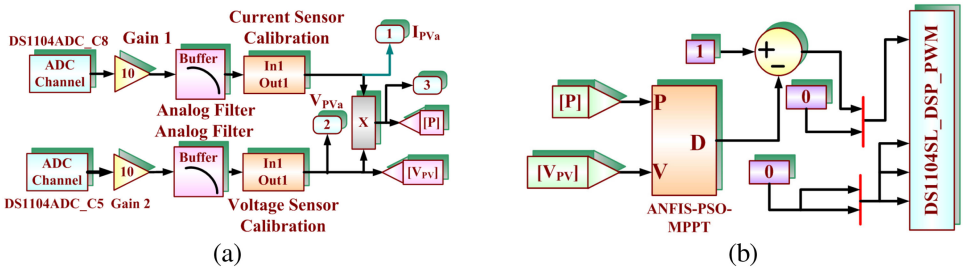

Fig. 10. Hybrid ANFIS–PSO-based MPPT controller design using dSPACE. (a) Instantaneous power. (b) PWM pulse generation.

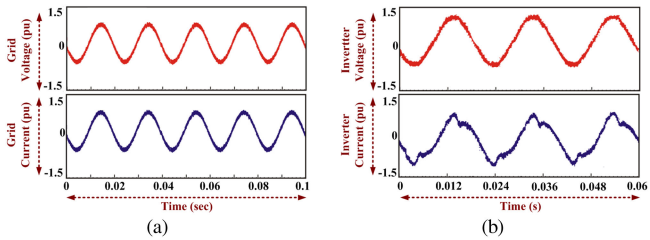

Fig. 11. Behavior of grid and inverter. (a) Grid behavior at unity power factor. (b) Inverter pursuance.

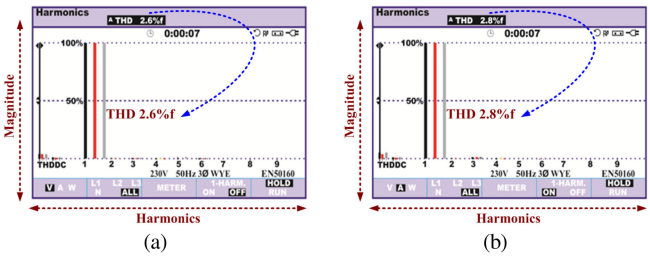

Fig. 12. FFT inverter performance (THD). (a) FFT of inverter output voltage. (b) FFT of inverter output current.

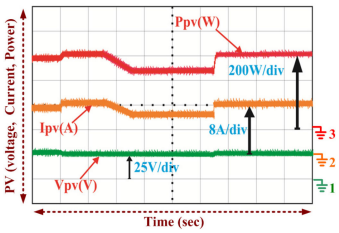

Fig. 13. Performance of hybrid ANFIS–PSO-based MPPT under changing solar insolation.

Using the dSPACE DS1104 platform, practical outcomes of PV voltage, current, and power are obtained that confirm the effectiveness of the hybrid ANFIS–PSO-based MPPT controller design as illustrated in Fig. 13. The experimental waveform with the proposed MPPT technique shown in Fig. 13 provides high accuracy and optimal PV power tracking under varying solar insolation. Fig. 14(a) and (b) depicts grid voltage and grid current waveforms under low to high solar insolation level and high to low solar insolation level, respectively. The practically

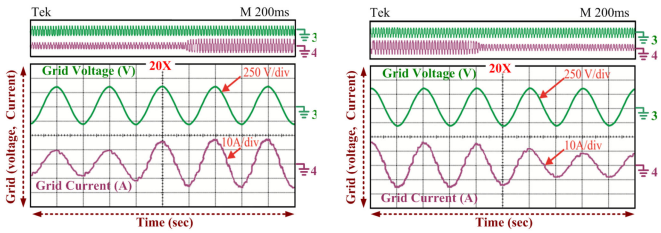

Fig. 14. Grid voltage and grid current waveforms under transient atmospheric conditions. (a) Low to high solar insolation level. (b) High to low solar insolation level.

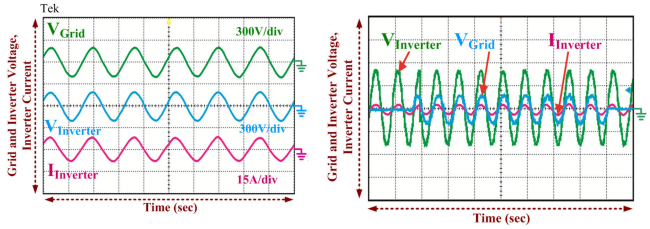

Fig. 15. Grid synchronization. (a) Inverter voltage, grid voltage, and inverter current under steady-state conditions. (b) Grid and inverter under dynamic operating conditions.

observed grid/current waveforms presented in Fig. 14(a) and (b), under transient atmospheric conditions, reveal the excellent performance of the proposed SVMHCC controller, in which grid current is in sinusoidal agreement with grid voltage having almost unity power coefficient. The experimental results shown in Fig. 15(a) and (b) reveal that inverter and grid are synchronized under steady and dynamic operating conditions. The behavior of an ANFIS–PSO MPPT algorithm has been tested under strong solar insolation profile presented in Fig. 16. The experimental Sun irradiance test profile is depicted in Fig. 16(a), which reveals that at $t = 1$ s, the level of Sun insolating values varies from 1000 to 400 W/m^2 and remains at 400 W/m^2 till $t = 5$ s. At $t = 5$ s, the solar irradiance level again becomes 1000 W/m^2.

Fig. 16(b) illustrates the power tracking ability of the proposed PV system with hybrid ANFIS–PSO MPPT control under the strong intensity of the Sun irradiance profile. The corresponding PV tracking power varies and is depicted in Fig. 16(b). The P&O

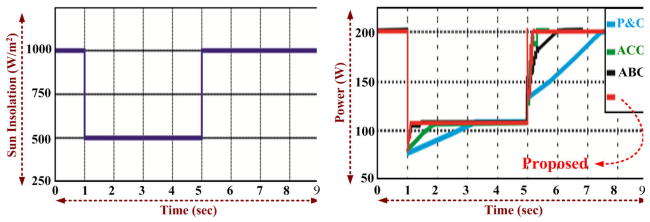

(a) (b)

Fig. 16. Power tracking ability in strong solar insolation profile. (a) Strong Sun insolation profile. (b) Power tracking ability of P&O, ACO, ABC, and ANFIS–PSO algorithms under strong Sun profile (simulation results).

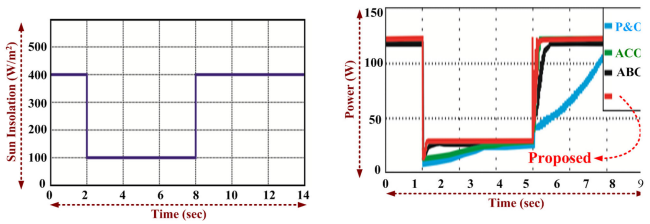

(a) (b)

Fig. 17. Power tracking ability in weak Sun insolation profile. (a) Strong Sun insolation profile. (b) Power tracking ability of P&O, ACO, ABC, and ANFIS–PSO algorithms under weak Sun profile (simulation results).

method has more oscillations around MPP and has long PV tracking power ability. The proposed hybrid ANFIS–PSO has excellent power tracking ability compared to the P&O, ACO, and ABC algorithms.

An ANFIS–PSO has the least MPP tracking period, zero oscillation around MPP, and low power losses. Also, the behavior of the ANFIS–PSO MPPT algorithm has been tested under weak solar insolation profile presented in Fig. 17(a). The solar insolation level is reduced from 400 to 100 W/m^2 at $t = 2$ s and remains constant till 8 s, and then becomes 400 W/m^2 at $t = 14$ s. Compared to the P&O, ACO, and ABC methods, the proposed ANFIS–PSO has the shortest PV tracking period and zero oscillation around MPP operating point, as illustrated in Fig. 17(b).

The MATLAB/Simulink-based Sun irradiance profile has been employed to test the behavior of MPPT algorithms used, such as P&O, ACO, ABC, and hybrid ANFIS–PSO, under strong and weak Sun profiles. The performances of these algorithms through realistic solar insolation profile have been tested and presented in Figs. 18 and 19 under partial shading conditions using the dSPACE platform. Figs. 18 and 19 explain the power tracking ability of the employed algorithms under partial shading situations with varying solar insolation and ambient temperature. Fig. 18(a) and (b) describes the performance of the proposed PV power system under partial shading conditions using PSO and ACO, respectively. Fig. 19(a) and (b) describes the performance of the proposed PV power system under partial shading conditions using ABC and ANFIS–PSO, respectively. The three patterns have been applied to test the behavior of

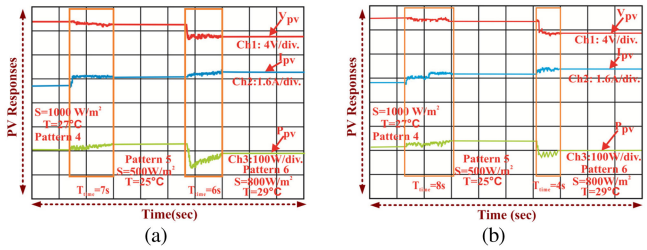

(a) (b)

Fig. 18. Power tracking ability of algorithms under partial shading conditions. (a) PSO. (b) ACO.

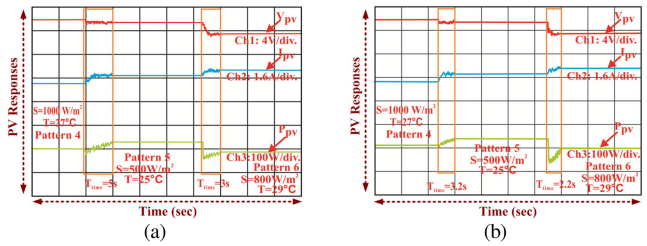

(a) (b)

Fig. 19. Power tracking ability of algorithms under partial shading conditions. (a) ABC. (b) ANFIS–PSO.

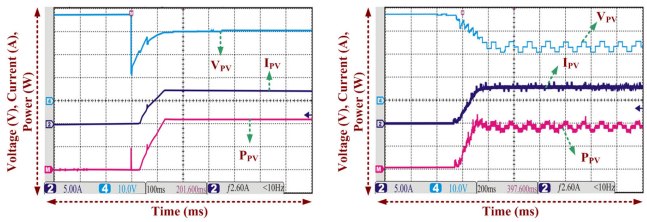

(a) (b)

Fig. 20. Power tracking ability of algorithms. (a) Proposed. (b) P&O.

the PSO, ACO, ABC, and proposed hybrid ANFIS–PSO MPPT algorithms.

It is revealed that the proposed hybrid ANFIS–PSO has the least PV tracking period to reach MPP compared to PSO-, ACO-, and ABC-based MPPT algorithms. The efficacy of the proposed hybrid ANFIS–PSO controller has been validated by comparison with the P&O method under changing solar insolation level, as presented in Fig. 20(a) and (b). Practical results interpret that the proposed hybrid ANFIS–PSO-based MPPT technique provides optimal PV power tracking with zero PV power disturbance near the MPP region compared to the P&O method. Furthermore, the proposed MPPT and inverter controller provide operation of unity power factor, which is realized through experimental results presented in Fig. 21. Fig. 22 depicts the plot of execution time versus the RMSE value presented using Table IV, which reveals that the proposed ANFIS–PSO algorithm has the least RMSE compared to other employed algorithms. The PSO algorithm provides proper training and updation to ANFIS variables. Mostly, the gradient approach has been employed for the determination of training parameters, which is strenuous, and chain rule produces local minima. Compared to the gradient

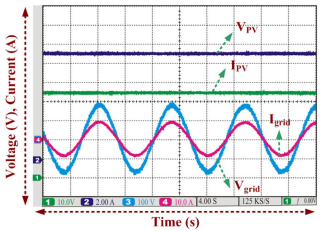

Fig. 21. PV responses at unity power factor operation.

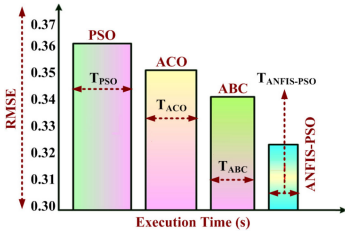

Fig. 22. Execution time versus RMSE.

TABLE IV
EXECUTION TIME VERSUS RMSE

Methods	Execution time	RMSE
PSO	0.9 sec (T_{PSO})	0.363
ACO	0.7 sec (T_{ACO})	0.352
ABC	0.65 sec (T_{ABC})	0.348
ANFIS-PSO	0.3 sec ($T_{ANFIS-PSO}$)	0.327

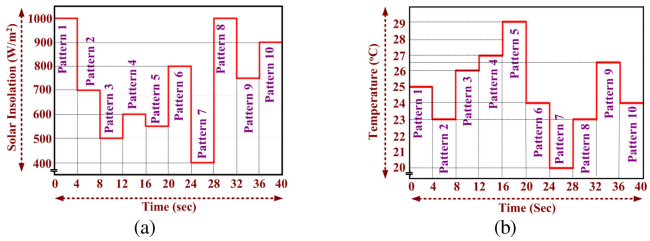

Fig. 23. Input variable 10 patterns of (a) solar insolations and (b) temperature.

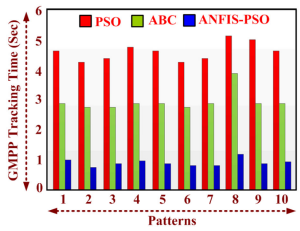

Fig. 24. PV tracking period using PSO, ABC, and ANFIS–PSO methods.

TABLE V
PV POWER TRACKING EFFICIENCY

Algorithms	Cycle				
	I	II	III	IV	Average
PSO	96.57	93.78	96.86	92.32	94.88
ABC	98.31	94.56	98.12	97.48	97.11
ANFIS-PSO (Proposed)	99.51	97.89	98.39	97.62	98.35

approach, the PSO technique provides rapid, simpler, and fast convergence for updating of ANFIS parameters. Moreover, the gradient method requires initial parameters for the calculation of learning rate. However, the PSO approach does not require learning rate calculation. Practical results reveal that the proposed hybrid ANFIS–PSO method has better responses for complex nonlinear systems equated with the conventional PSO method. Compared to other training techniques such as PSO, ACO, and ABC, the proposed hybrid ANFIS–PSO has better PV power tracking ability, least RMSE execution period, and free derivation for finding antecedent parameters for proper training under uniform, nonuniform, and partial shading conditions.

An Agilent PV simulator is employed to provide emulation of the PV power system and vary the solar insolation levels. With the help of the PV simulator, the values of Sun insolation vary from 1000 to 400 W/m^2 and temperature at this moment is kept constant at 25 °C. However, when solar radiation changes, the temperature of the system also varies. In this article, authors have evaluated the performance of the proposed PV power system under changing solar irradiance as well as temperature and PV tracking periods for PSO, ABC, and ANFIS–PSO algorithms have been calculated. Fig. 23 depicts the input variable 10 patterns of solar insolations as well as temperature applied to the PV power system, and the PV tracking period is calculated, which is presented in Fig. 24. Fig. 25 presents the output of PV power using the PSO-, ABC-, and ANFIS–PSO-based MPPT methods. Experimental results reveal that the proposed ANFIS–PSO MPPT has very low PV tracking period to achieve MPP. It also concludes that the ANFIS–PSO performs rapid PV tracking compared to the PSO and ABC algorithms and has less power loss, high PV tracking efficiency, and least PV tracking time to obtain global MPP.

Moreover, the performance of the employed ANFIS–PSO algorithm has been validated by the calculation of real-time efficiency of the PV power system presented in Table V and with results shown in Fig. 26. The dynamic efficiency of the PV power system using the Agilent PV simulator is calculated mathematically as

$$\eta_{\text{dynamic MPPT}} = \frac{\int_0^{M_P} P_{\text{PV}}(T)dT}{\int_0^{M_P} P_{\text{MPP}}(T)dT} \tag{15}$$

where $P_{\text{PV}}(T)$ is the power extracted from the PV module, $P_{\text{MPP}}(T)$ is the PV power at MPP, and M_P is the total measured time.

The behavior of PSO, ABC, and proposed ANFIS–PSO has been evaluated under varying weather conditions in Fig. 26 and the presented results strongly reveal that the proposed ANFIS–PSO-based MPPT provides high PV tracking efficiency and has zero power oscillations around the global MPP region. Table V describes the numerical values of average tracking efficiencies of the PSO, ABC, and ANFIS–PSO algorithms under different operating cycles. Fig. 27 presents the PV tracking behavior of the proposed PV power system using the PSO-, ABC-, and ANFIS–PSO-based MPPT algorithms. The proposed ANFIS–PSO algorithm tracks MPP in every pattern efficiently with less

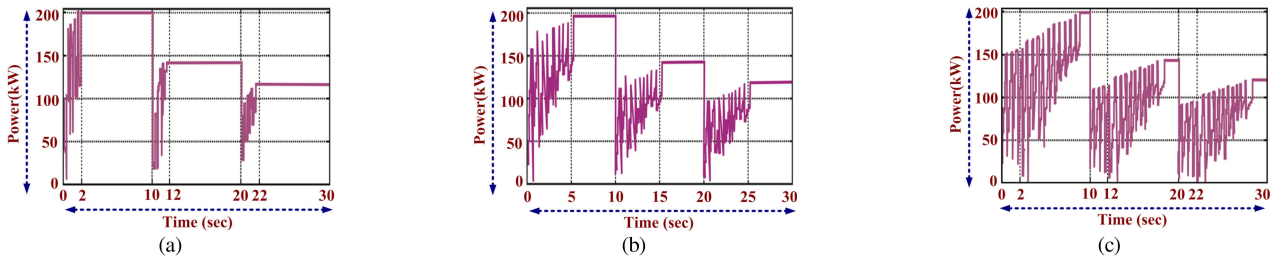

Fig. 25. PV tracking power capability using algorithms. (a) Proposed ANFIS–PSO. (b) ABC. (c) PSO.

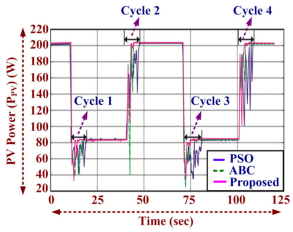

Fig. 26. Comparison of behavior of PSO, ABC, and proposed ANFIS–PSO under varying weather conditions.

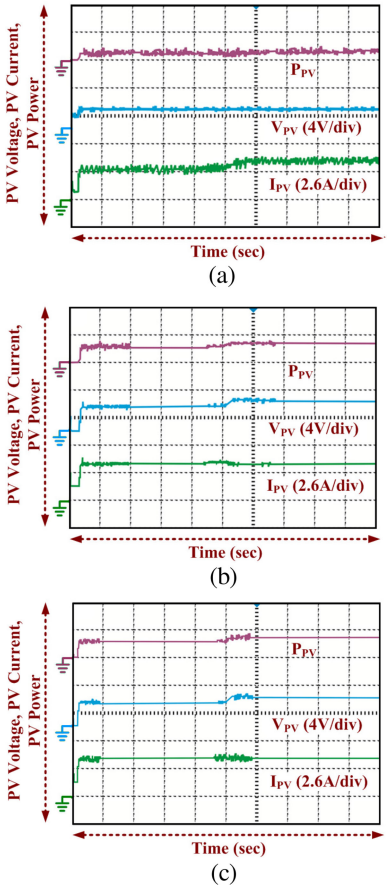

Fig. 27. PV tracking power using algorithms. (a) PSO. (b) ABC. (c) ANFIS–PSO.

tracking period. The employed ANFIS–PSO-based MPPT has rapid convergence velocity, high PV tracking efficiency, and lesser power loss ability and is able to achieve quick MPP region compared to ABC- and PSO-based MPPT methods.

V. Conclusion

In this article, experimental justification of a hybrid ANFIS–PSO and SVMHCC inverter control has been provided for the achievement of PV MPPT as well as injection of sinusoidal current to the electric grid. Compared to execution periods to obtain the least RMSE using PSO, ACO, and ABC, the proposed hybrid ANFIS–PSO has the least execution time (0.30 s), which justifies the acceptance of MPPT controller design. Inverter-fed sinusoidal current with low total harmonic distortion (THD) followed the IEEE 519 standard. A Zeta converter provides zero ripple output with MPPT functions using the proposed hybrid methodology. The performance of the proposed MPPT is commensurate with P&O, ACO, and ABC MPPT methods that provide rapid, precise, and accurate PV tracking under fluctuating weather conditions. It is revealed that the PV power system is functioning with zero steady-state error and has rapid PV tracking convergence velocity under highly fluctuating Sun insolation, which is validated through practical responses. Compared to other training techniques such as PSO, ACO, and ABC, the proposed hybrid ANFIS–PSO has better PV power tracking ability, least RMSE execution period, and free derivation for finding antecedent parameters for proper training under uniform, nonuniform, and partial shading conditions. The obtained experimental results correspond to standard grid codes for the grid-tied PV system. The main contributions to academic field knowledge and industrial sectors' experience on the real platform are to obtain the best MPPT configuration based on the hybrid ANFIS–PSO algorithm and have the least execution time, which justifies the acceptance of MPPT controller design. Moreover, the obtained experimental results explain achievement of PV MPPT as well as injection of sinusoidal current to the electric grid and that the PV power system is functioning with zero steady-state error and has rapid PV tracking convergence velocity under highly fluctuating Sun insolation. The implemented work can be extended with multilevel inverter topology as well as the Internet of Things-based MPPT control strategies as a future scope.

References

[1] J. R. R. Zientarski, M. L. D. S. Martins, J. R. Pinheiro, and H. L. Hey, "Series-connected partial-power converters applied to PV systems: A design approach based on step-up/down voltage regulation range," *IEEE Trans. Power Electron.*, vol. 33, no. 9, pp. 7622–7633, Sep. 2018.

[2] N. Priyadarshi, S. Padmanaban, M. S. Bhaskar, F. Blaabjerg, and A. Sharma, "Fuzzy SVPWM-based inverter control realisation of grid integrated photovoltaic–wind system with fuzzy particle swarm optimisation maximum power point tracking algorithm for a grid-connected PV/wind power generation system: Hardware implementation," *IET Elect. Power Appl.*, vol. 12, no. 7, pp. 962–971, Aug. 2018.

[3] A. Sangwongwanich, Y. Yang, F. Blaabjerg, and D. Sera, "Delta power control strategy for multistring grid-connected PV inverters," *IEEE Trans. Ind. Appl.*, vol. 53, no. 4, pp. 3862–3870, Jul./Aug. 2017.

[4] M. Jedari and S. H. Fathi, "A new approach for photovoltaic arrays modeling and maximum power point estimation in real operating conditions," *IEEE Trans. Ind. Electron.*, vol. 64, no. 12, pp. 9334–9343, Dec. 2017.

[5] F. E. Aamri, H. Maker, D. Sera, S. V. Spataru, J. M. Guerrero, and A. Mouhsen, "A direct maximum power point tracking method for single-phase grid-connected PV inverters," *IEEE Trans. Power Electron.*, vol. 33, no. 10, pp. 8961–8971, Oct. 2018.

[6] A. Souza, F. C. Melo, T. L. Oliveira, and C. E. Tavares, "Performance analysis of the computational implementation of a simplified PV model and MPPT algorithm," *IEEE Latin Amer. Trans.*, vol. 14, no. 2, pp. 792–798, Feb. 2016.

[7] O. Khan, S. Acharya, M. A. Hosani, and M. S. E. Moursi, "Hill climbing power flow algorithm for hybrid DC/AC microgrids," *IEEE Trans. Power Electron.*, vol. 33, no. 7, pp. 5532–5537, Jul. 2018.

[8] D. C. Huynh and M. W. Dunnigan, "Development and comparison of an improved incremental conductance algorithm for tracking the MPP of a solar PV panel," *IEEE Trans. Sustain. Energy*, vol. 7, no. 4, pp. 1421–1429, Oct. 2016.

[9] N. Kumar, I. Hussain, B. Singh, and B. K. Panigrahi, "Framework of maximum power extraction from solar PV panel using self predictive perturb and observe algorithm," *IEEE Trans. Sustain. Energy*, vol. 9, no. 2, pp. 895–903, Apr. 2018.

[10] A. G. Al-Gizi, A. Craciunescu, and S. J. Al-Chlaihawi, "The use of ANN to supervise the PV MPPT based on FLC," in *Proc. 10th Int. Symp. Adv. Topics Elect. Eng*, Bucharest, Romania, Mar. 23–25, 2017, pp. 703–708.

[11] H. Abu-Rub, A. Iqbal, S. M. Ahmed, F. Z. Peng, Y. Li, and G. Baoming, "Quasi-Z-source inverter-based photovoltaic generation system with maximum power tracking control using ANFIS," *IEEE Trans. Sustain. Energy*, vol. 4, no. 1, pp. 11–20, Jan. 2013.

[12] R. B. A. Koad, A. F. Zobaa, and A. El-Shahat, "A novel MPPT algorithm based on particle swarm optimization for photovoltaic systems," *IEEE Trans. Sustain. Energy*, vol. 8, no. 2, pp. 468–476, Apr. 2017.

[13] N. A. Windarko, A. Tjahjono, D. O. Anggriawan, and M. H. Purnomo, "Maximum power point tracking of photovoltaic system using adaptive modified firefly algorithm," in *Proc. Int. Electron. Symp.*, Surabaya, Indonesia, Sep. 29–30, 2015, pp. 31–35.

[14] K. Sundareswaran, V. Vigneshkumar, P. Sankar, S. P. Simon, P. S. R. Nayak, and S. Palani, "Development of an improved P&O algorithm assisted through a colony of foraging ants for MPPT in PV system," *IEEE Trans. Ind. Inform.*, vol. 12, no. 1, pp. 187–200, Feb. 2016.

[15] K. Sundareswaran, P. Sankar, P. S. R. Nayak, S. P. Simon, and S. Palani, "Enhanced energy output from a PV system under partial shaded conditions through artificial bee colony," *IEEE Trans. Sustain. Energy*, vol. 6, no. 1, pp. 198–209, Jan. 2015.

[16] N. Priyadarshi, S. Padmanaban, P. K. Maroti, and A. Sharma, "An extensive practical investigation of FPSO-based MPPT for grid integrated PV system under variable operating conditions with anti-islanding protection," *IEEE Syst. J.*, vol. 13, no. 2, pp. 1861–1871, Jun. 2019.

[17] R. Kumar and B. Singh, "BLDC motor-driven solar PV array-fed water pumping system employing zeta converter," *IEEE Trans. Ind. Appl.*, vol. 52, no. 3, pp. 2315–2322, May/Jun. 2016.

[18] A. Lashab, D. Sera, J. M. Guerrero, L. Mathe, and A. Bouzid, "Discrete model-predictive-control-based maximum power point tracking for PV systems: Overview and evaluation," *IEEE Trans. Power Electron.*, vol. 33, no. 8, pp. 7273–7287, Aug. 2018.

[19] W. Wang, J. Zhang, and M. Cheng, "A dual-level hysteresis current control for one five-leg VSI to control two PMSMs," *IEEE Trans. Power Electron.*, vol. 32, no. 1, pp. 804–814, Jan. 2017.

[20] E. A. R. E. Ariff, O. Dordevic, and M. Jones, "A space vector PWM technique for a three-level symmetrical six-phase drive," *IEEE Trans. Ind. Electron.*, vol. 64, no. 11, pp. 8396–8405, Nov. 2017.

[21] M. Mir, M. Kamyab, M. J. Lariche, A. Bemani, and A. Baghban, "Applying ANFIS–PSO algorithm as a novel accurate approach for prediction of gas density," *Petroleum Sci. Technol.*, vol. 36, no. 12, pp. 820–826, Jun. 2018.

[22] H. Darvish, S. Rahmani, A. M. Sadeghi, and M. H. E. Baghdadi, "The ANFIS–PSO strategy as a novel method to predict interfacial tension of hydrocarbons and brine," *Petroleum Sci. Technol.*, vol. 36, no. 9–10, pp. 654–659, May 2018.

[23] Y. K. Semero, J. Zhang, and D. Zheng, "PV power forecasting using an integrated GA–PSO–ANFIS approach and Gaussian process regression based feature selection strategy," *CSEE J. Power Energy Syst.*, vol. 4, no. 2, pp. 210–218, Jun. 2018.

[24] Y. K. Semero, D. Zheng, and J. Zhang, "A PSO–ANFIS based hybrid approach for short term PV power prediction in microgrids," *Elect. Power Compon. Syst.*, vol. 46, no. 1, pp. 95–103, Jan. 2018.

[25] M. Bagheri, V. Nurmanova, O. Abedinia, and M. S. Naderi, "Enhancing power quality in microgrids with a new online control strategy for DSTATCOM using reinforcement learning algorithm," *IEEE Access*, vol. 8, pp. 38986–38996, Jul. 2018.

[26] O. Abedinia, M.S. Naderi, A. Jalili, and A. Mokhtarpour, "A novel hybrid GA–PSO technique for optimal tuning of fuzzy controller to improve multi-machine power system stability," *Int. Rev. Elect. Eng.*, vol. 6. no. 2, pp. 863–873, Mar. 2011.

[27] L. P. Ling and N. A. Azli, "SVM based hysteresis current controller for a three phase active power filter," in *Proc. Nat. Power Energy Conf.*, Kuala Lumpur, Malaysia, Nov. 29–30, 2004, pp. 132–136.

Neeraj Priyadarshi received the M.Tech. degree in power electronics and drives from the Vellore Institute of Technology (VIT), Vellore, India, in 2010, and the Ph.D. degree from the Government College of Technology and Engineering, Udaipur, Rajasthan, India, in 2015.

He is currently with MIT, Purnea, India. He was previously with the JK University, Geetanjali Institute, Global Institute, and SS Group, Rajasthan, India. He has authored or coauthored more than 40 papers in journals and conferences. His current research interests include power electronics, control system, power quality, and solar power generation.

Dr. Priyadarshi is a Reviewer of the *International Journal of Renewable Energy Research*.

Sanjeevikumar Padmanaban (M'12–SM'15) received the bachelor's degree in electrical engineering from the University of Madras, Chennai, India, in 2002, the master's degree (Hons.) in electrical engineering from Pondicherry University, Puducherry, India, in 2006, and the Ph.D. degree in electrical engineering from the University of Bologna, Bologna, Italy, in 2012.

He was an Associate Professor with VIT University from 2012 to 2013. In 2013, he joined the National Institute of Technology, India, as a Faculty Member. In 2014, he was invited as a Visiting Researcher at the Department of Electrical Engineering, Qatar University, Doha, Qatar, funded by the Qatar National Research Foundation (Government of Qatar). He continued his research activities with the Dublin Institute of Technology, Dublin, Ireland, in 2014. He was an Associate Professor with the Department of Electrical and Electronics Engineering, University of Johannesburg, Johannesburg, South Africa, from 2016 to 2018. Since 2018, he has been a Faculty Member with the Department of Energy Technology, Aalborg University, Esbjerg, Denmark. He has authored more than 300 scientific papers.

Dr. Padmanaban was the recipient of the Best Paper cum Most Excellence Research Paper Award from IET-SEISCON'13, IET-CEAT'16, IEEE-EECSI'19, IEEE-CENCON'19 and five best paper awards from ETAEERE'16 sponsored Lecture Notes in Electrical Engineering, Springer book series. He is a Fellow of the Institution of Engineers, India, the Institution of Electronics and Telecommunication Engineers, India, and the Institution of Engineering and Technology, U.K. He is an Editor/Associate Editor/Editorial Board for refereed journals, in particular the IEEE SYSTEMS JOURNAL, IEEE ACCESS, *IET Power Electronics*, and *Journal of Power Electronics* (Korea), and the Subject Editor for the *IET Renewable Power Generation*, *IET Generation, Transmission and Distribution*, and *FACTS* journal (Canada).

Jens Bo Holm-Nielsen received the M.Sc. degree in agricultural systems, crops, and soil science from KVL, Royal Veterinary and Agricultural University, Copenhagen, Denmark, in 1980, and the Ph.D. degree in process analytical technologies for biogas Systems with Aalborg University, Esbjerg, Denmark, in 2008.

He is currently with the Department of Energy Technology, Aalborg University, Esbjerg, Denmark, and is the Head of the Esbjerg Energy Section. He is also the Head of the research group with the Center for Bioenergy and Green Engineering established in 2009. He has vast experience in the field of biorefinery concepts and biogas production–anaerobic digestion. He has implemented projects of bioenergy systems in Denmark with provinces and European states. He was the Technical Advisor for many industries in this field. He has executed many large-scale European Union and United Nation projects in research aspects of bioenergy, biorefinery processes, and the full chain of biogas and green engineering. He has authored more than 300 scientific papers. His current research interests include renewable energy, sustainability, and green jobs for all.

Dr. Holm-Nielsen was a member on invitation with various capacities in the committee for more than 500 various international conferences and an organizer of international conferences, workshops, and training programs in Europe, Central Asia, and China.

Frede Blaabjerg (S'86–M'88–SM'97–F'03) received the Ph.D. degree in electrical engineering from Aalborg University, Aalborg, Denmark, in 1995.

He was with ABB-Scandia, Randers, Denmark, from 1987 to 1988. From 1988 to 1992, he was with Aalborg University. He was an Assistant Professor in 1992, an Associate Professor in 1996, and a Full Professor of power electronics and drives in 1998. Since 2017, he has been a Villum Investigator. He is an honoris causa at University Politehnica Timisoara, Romania and Tallinn Technical University, Estonia. He has authored or coauthored more than 600 journal papers in the fields of power electronics and its applications. He is the coauthor of four monographs and editor of 10 books in power electronics and its applications. His current research interests include power electronics and its applications such as in wind turbines, PV systems, reliability, harmonics, and adjustable speed drives.

Dr. Blaabjerg was the recipient of the 30 IEEE Prize Paper Awards, the IEEE PELS distinguished Service Award in 2009, the EPE-PEMC Council Award in 2010, the IEEE William E. Newell Power Electronics Award 2014, and the Villum Kann Rasmussen Research Award 2014. He was the Editor-in-Chief for the IEEE TRANSACTIONS ON POWER ELECTRONICS from 2006 to 2012. He was a Distinguished Lecturer for the IEEE Power Electronics Society from 2005 to 2007 and for the IEEE Industry Applications Society from 2010 to 2011 as well as from 2017 to 2018. For the period of 2019–2020, he is the President of IEEE Power Electronics Society. He is the Vice-President of the Danish Academy of Technical Sciences. He has been nominated in 2014–2018 by Thomson Reuters to be among the 250 most cited researchers in engineering around the world.

Mahajan Sagar Bhaskar (M'15) received the bachelor's degree in electronics and telecommunication engineering from the University of Mumbai, Mumbai, India, in 2011, and the master's degree in power electronics and drives from the Vellore Institute of Technology, VIT University, Vellore, India, in 2014, and the Ph.D. degree in electrical and electronic engineering form the University of Johannesburg, Johannesburg, South Africa, in 2019.

He is currently with Renewable Energy Laboratory, Department of Communications and Networks Engineering, College of Engineering, Prince Sultan University, Riyadh, Saudi Arabia. He was a Researcher Assistant with the Department of Electrical Engineering, Qatar University, Doha, Qatar. He was as an Assistant Professor and a Research Coordinator with the Department of Electrical and Electronics Engineering, Marathwada Institute of Technology (MIT), Aurangabad, India. He has authored/coauthored scientific papers in the field of power electronics, with particular reference to XY converter family, multilevel dc/dc and dc/ac converter, and high-gain converter. He has authored over 100 scientific papers.

Dr. Bhaskar is a member of IEEE Industrial Electronics Society, IEEE Power Electronics, IEEE Industrial Applications Society, and IEEE Power and Energy Society, IEEE Robotics and Automation Society, IEEE Vehicular Technology Society, Young Professionals, various IEEE Councils and Technical Communities. He is a reviewer member of various international journals and conferences including IEEE and IET and has received the Best Paper Research Paper Award from IEEE-CENCON'19, IEEE-ICCPCT'14, IET-CEAT'16, and ETAEERE'16 sponsored Lecture note in Electrical Engineering, Springer book series. He is the recipient of the IEEE Access award "Reviewer of Month" in January 2019 for his valuable and thorough feedback on manuscripts, and for his quick turnaround on reviews.